

Formation and migration of oxygen and zirconium vacancies in cubic zirconia and zirconium oxysulfide

Oleksandr I. Malyi ^a, Ping Wu ^{a,b,*}, Vadym V. Kulish ^a, Kewu Bai ^c, Zhong Chen ^{a,*}

^a School of Materials Science and Engineering, Nanyang Technological University, 50 Nanyang Avenue, Singapore 639798, Singapore

^b Engineering Product Development, Singapore University of Technology and Design, 20 Dover Drive, Singapore 138682, Singapore

^c Institute of High Performance Computing, 1 Fusionopolis Way, 16–16 Connexis, Singapore 138632, Singapore

ARTICLE INFO

Article history:

Received 8 December 2011

Received in revised form 20 January 2012

Accepted 21 January 2012

Available online 24 February 2012

Keywords:

Vacancy

Migration barrier

Density functional theory

Ionic conductivity

ABSTRACT

Oxygen ionic conductivity through zirconia (ZrO_2) is essential to the performance of solid oxide fuel cells, thermal barrier coatings, and zirconium alloys for nuclear fuel cladding. Since sulfur (S) atoms can replace oxygen atoms at ZrO_2 surface or even induce formation of homogeneous zirconium oxysulfide (ZrOS) structure at high S partial pressure, we study defect migration and formation in both cubic zirconia (c- ZrO_2) and ZrOS under different electron and element chemical potentials using density functional theory. Our calculations show that S addition to zirconia, either by doping or through gas diffusion, increases both the formation energy and migration barrier of doubly positively charged oxygen vacancies. Since the charged oxygen vacancies play a vital role in the ionic and thermal conductivities, our results suggest that high S partial pressures are expected to change the mechanisms of ionic and thermal conductivities of ZrO_2 -based materials.

© 2012 Elsevier B.V. All rights reserved.

1. Introduction

In the past decades, zirconia (ZrO_2) has emerged as an important material system for gas sensors [1], high-temperature electrolysis [2], thermal barrier coatings [3], solid oxide fuel cells (SOFCs) [4–7], etc. For instance, nanocrystalline ZrO_2 – CeO_2 solid solutions and Cu/ CeO_2 /yttria doped zirconia (YDZ) are one of the most promising anode materials for SOFCs operating on hydrocarbon fuels [8,9]. It is well known that three zirconia polymorphs can exist at atmospheric pressure, namely: monoclinic (m- ZrO_2), tetragonal (t- ZrO_2) and cubic (c- ZrO_2) [10–12]. In practice, it is more attractive to use oxide-doped ZrO_2 systems, since addition of yttria (Y_2O_3) to ZrO_2 increases the concentration of oxygen vacancies and, consequently, significantly increases its ionic conductivity [13–15]. Despite this, a number of recent publications report investigations of properties of undoped zirconia polymorphs [10,12,16–29]. On the one hand, such studies can provide information on the chemistry of pure zirconia. On the other hand, most of the properties of yttria-doped zirconia (<40 mol% Y_2O_3) can generally be considered as a superposition of the properties of c- ZrO_2 and $Y_4Zr_3O_{12}$ domains [15,30,31], therefore such studies are the basis for understanding of YDZ properties.

Since defects, especially the lattice vacancies, have a major impact on the performance of the ZrO_2 -based devices, a lot of theoretical researches have been devoted to the investigation of their effects on the

atomic and electronic structures of different zirconia phases [9,11,15–28]. Several works have also been focused on the role of oxygen vacancies in the stabilization of c- ZrO_2 and t- ZrO_2 structures at low temperatures [14,15,30,32–36]. Nevertheless, all these studies were limited to the investigation of pure ZrO_2 systems or ZrO_2 with a low concentration of oxide additions (MgO, Y_2O_3 , and CaO). In fact, doped and undoped ZrO_2 as well as oxidation (corrosion) of zirconium (or zirconium alloys) can be affected by environmental conditions. For instance, at high sulfur (S) partial pressure S atoms can replace oxygen atoms at ZrO_2 surface, or induce coexistence of ZrO_2 and zirconium oxysulfide (ZrOS) structures or even formation of homogeneous ZrOS structure (P213 space group, see Fig. 1a) [28,37,38]. Hence, it becomes clear that transition between ZrO_2 and ZrOS phases can change system properties; however, no studies on this topic have been reported so far. Therefore, we report density functional theory (DFT) calculations on the migration of oxygen vacancies in c- ZrO_2 and ZrOS and on the formation of oxygen and zirconium vacancies in these structures under different electron and element chemical potentials.

In this paper, undoped c- ZrO_2 (Fm3m, see Fig. 1b) was chosen for the defect calculations in zirconia. It is noteworthy that formation energies of intrinsic vacancies in cubic, tetragonal, and monoclinic zirconia polymorphs are close to each other [21,23,24,26,27,39]. Besides, since the lowest migration barrier of oxygen vacancy in YDZ corresponds to the configuration where oxygen vacancy is placed far away from yttrium ions [14,34,35,40,41], migration barrier of doubly positively charged oxygen vacancy (V_O^{2+}) in c- ZrO_2 can be directly compared with that in YDZ. Therefore, our study not only enhances current understanding of sulfur poisoning of zirconia and SOFC anode materials, but also provides

* Corresponding authors.

E-mail addresses: wuping@sutd.edu.sg (P. Wu), ASZChen@ntu.edu.sg (Z. Chen).

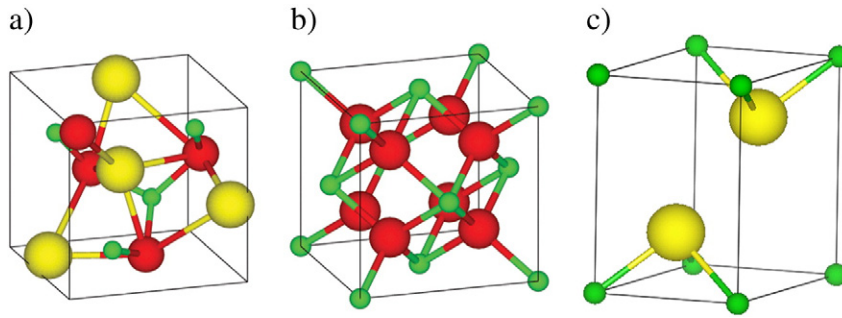


Fig. 1. Structures of (a) ZrOS, (b) cubic ZrO₂, and (c) ZrS₂. The red spheres are O ions, green spheres are Zr ions, and yellow spheres are S ions.

guidance for the development of new materials for gas sensing, high-temperature electrolysis, thermal barrier coatings and SOFCs.

2. Methodology

The first-principles calculations were carried out within the DFT framework using Perdew-Burke-Ernzerhof (PBE) functional [42] and the plane-wave pseudopotential method as implemented in the Quantum-Espresso package [43]. The ultrasoft pseudopotentials [44] with $2s^2 2p^4$, $3s^2 3p^4$, $4s^2 4p^6 4d^2 5s^2$ as the valence electron configurations for the oxygen, sulfur and zirconium, respectively, were used for the description of electron-ion interactions. A Monkhorst-Pack mesh [45] with $10 \times 10 \times 10$ k-point sampling was employed for prediction of equilibrium lattice constants of c-ZrO₂, ZrOS, and ZrS₂ (P-3m1, see Fig. 1c [46]) structures, while for defect calculations $4 \times 4 \times 4$ k-point sampling was used. Before any structure relaxation and property calculation the converging tests were performed from which the plane-wave kinetic energy and charge density cutoffs were set as 50 Ry and 600 Ry, respectively, for all simulations reported here.

Point defect calculations in both c-ZrO₂ and ZrOS structures were performed in supercells containing 96 atoms. All atoms in the supercells were relaxed without changing the lattice parameters by using the Broyden-Fletcher-Goldfarb-Shanno (BFGS) method until the maximum force on each atom was less than 0.01 eV/Å. The formation energy of a point defect ($\Delta H_{D,q}$) in charge state q was calculated by [47]

$$\Delta H_{D,q}(E_f, \mu) = (E_{D,q} - E_H) + q(E_{VBM} + E_f + \Delta V) + \mu_i \quad (1)$$

where $E_{D,q}$ is the total energy of the supercell containing the point defect; E_H is the total energy of the perfect system. The second term describes the dependence on the Fermi level (E_f) measured from the valence band edge, E_{VBM} is a position of the valence band maximum (VBM) in the perfect system, and ΔV aligns the VBM in the defect and perfect crystal supercells. The chemical potentials of the constituents are given by the third term, where μ_i can be rewritten as $\mu_i = \mu_i^{ref} + \Delta\mu_i$. μ_i^{ref} was calculated for the reference materials including zirconium (P63/mmc), sulfur (Fddd) and oxygen (isolated molecule stored in a large box with dimensions $20 \times 20 \times 20 \text{ \AA}^3$). It should also be noted that although the finite supercell size may contribute interaction between charged defect and its periodic images, we did not use Makov-Payne model [48] for the correction of the total energy of the charged systems, since this model significantly overestimates the correction for image charge interactions in zirconia [27].

Calculations of migration barriers and predictions of the minimum energy pathways of the vacancy hopping were carried out by using the nudged elastic band (NEB) method [49,50]. Initial guesses of the vacancy migration pathways were generated by linear interpolations (with nine images) between initial and final points of vacancy jumps. Unlike the calculations of defect formation energies and DOS, migration energies of defects are obtained by calculating the energy differences

between configurations (saddle point and lowest energy state) which are structurally and electronically very similar. Therefore, this type of calculations is less sensitive to errors, consequently, calculations of the migration barriers were performed with less number of k-points ($2 \times 2 \times 2$ k-point sampling). In this work, we did not consider migration of zirconium vacancies because we believe that they cannot provide conduction in ZrO₂-based materials. For the oxygen vacancies our calculations have been limited to the study of the migration of V_O^{+2} vacancies, since this type of vacancies has the lowest migration barrier and plays a central role in the ionic conductivity of both pure and oxide-doped zirconia [14,24].

3. Results and discussion

3.1. Atomic structures, stability diagram and elemental chemical potentials

First, we perform analysis of c-ZrO₂, ZrOS, and ZrS₂ structures. On the one hand, it can provide information on different types of oxygen vacancies existing in c-ZrO₂ and ZrOS structures. On the other hand, in order to derive defect formation energies ($\Delta H_{D,q}$), the thermodynamic conditions ($\Delta\mu_o$, $\Delta\mu_s$ and $\Delta\mu_{Zr}$) need to be defined. The calculated structural parameters of c-ZrO₂, ZrOS, and ZrS₂ structures, listed in Table 1, agree well with experimental data, but show the small consistent overestimations common for GGA. Unlike m-ZrO₂, where two types of oxygen atoms exist (fourfold and threefold coordinated oxygen) [23], only one type of oxygen ions exists in c-ZrO₂ and ZrOS structures (for more details see [16,37]). The predicted band gap of c-ZrO₂ is 3.3 eV, it is smaller than the experimental values (5.4 eV - 5.7 eV) [51], but agrees with other first-principles studies [21,26–28,39,52,53]. For ZrOS structure the predicted band gap is 2.5 eV, which also agrees well with that calculated by using Wien2k software.[28]

Predictions of the thermodynamic conditions ($\Delta\mu_o$, $\Delta\mu_s$, and $\Delta\mu_{Zr}$) were carried out by using well defined methodology [10,21,26,27,47,54–57]. For c-ZrO₂ at the thermodynamic equilibrium (at the low sulfur partial pressure), its chemical potential can be calculated from

$$\mu_{c-ZrO_2} = \mu_{Zr}^{bulk} + 2\mu_o^{gas} + \Delta H_{c-ZrO_2} \quad (2)$$

where ΔH_{c-ZrO_2} is the formation heat of c-ZrO₂ calculated from DFT calculations (in this work $\Delta H_{c-ZrO_2} = -11.97$ eV). In addition, to suspend the

Table 1

Lattice parameters (in Å) and formation heats (in eV) for c-ZrO₂, ZrOS and ZrS₂. Present results are compared with experimental data.

	Lattice parameters (in Å)		Formation energies (in eV)	
	This work	Experiment	This work	Experiment
c-ZrO ₂	5.106	5.090[16]	-11.97	-11.12[62]
ZrOS	5.719	5.696[37]	-8.55	-7.88[62]
ZrS ₂	3.680	3.662[46]	-4.70	-
	5.858	5.826[46]		

formation of bulk zirconium and oxygen gas condition (3) has to be conserved (otherwise the oxide is unstable).

$$\Delta\mu_{Zr} = \mu_{Zr} - \mu_{Zr}^{bulk} \leq 0 \text{ and } \Delta\mu_O = \mu_O - E_{O_2^{gas}}/2 \leq 0 \quad (3)$$

For the thermodynamically stable ZrOS, the variations of elemental chemical potentials ($\Delta\mu_i$) are restricted by Eq.(4) and formation of competing phases such as c-ZrO₂ or ZrS₂ according to Eqs. (5), (6)

$$\Delta H_{ZrOS} = \Delta\mu_{Zr} + \Delta\mu_O + \Delta\mu_S \quad (4)$$

$$\Delta H_{c-ZrO_2} = \Delta\mu_{Zr} + 2\Delta\mu_O \quad (5)$$

$$\Delta H_{ZrS_2} = \Delta\mu_{Zr} + 2\Delta\mu_S \quad (6)$$

where ΔH_{ZrOS} , and ΔH_{ZrS_2} are calculated formation heats of ZrOS (−8.55 eV), and ZrS₂ (−4.70 eV), respectively. These conditions determine the phase diagram shown in Fig. 2. It can be seen that undoped zirconia is thermodynamically stable over a wide range of chemical potentials. However, the combination of low oxygen and high sulfur partial pressures may result in the stabilization of ZrOS. In Fig. 2 the gray shaded area represents the chemical stability range of ZrOS. It should be noted that line through points C and D (calculated by using Eqs. 4 and 6) corresponds to coexistence conditions of ZrOS and ZrS₂ structures. Whereas, line through points A and B (calculated by using Eqs. 4, and 5) corresponds to the coexistence conditions of c-ZrO₂ and ZrOS structures. Based on these results, the defect calculations have been performed for two extreme conditions: oxygen-rich limit (point A, $\Delta\mu_O = -3.42$ eV) and oxygen-poor limit (point B, $\Delta\mu_O = -5.99$ eV). This range of oxygen chemical potential ($\Delta\mu_O$) is different from that for c-ZrO₂ at low sulfur partial pressure ($0 \text{ eV} > \Delta\mu_O > H_{c-ZrO_2}/2$), therefore our results under oxygen-rich limit cannot be compared with previously reported data.

3.2. Formation of zirconium and oxygen vacancies in ZrOS and c-ZrO₂ structures

Details of the atomistic displacements (with reference to the perfect crystals) surrounding different vacancies in both bulk c-ZrO₂ and ZrOS are shown in Table 2, where NN_{Zr} (NN_O, and NN_S) is the

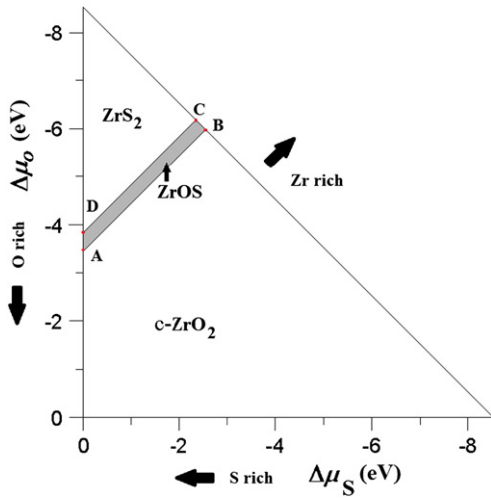


Fig. 2. Stability diagram for ZrOS as determined from DFT calculations. The area confined between points A ($\Delta\mu_O = -3.42$ eV, $\Delta\mu_{Zr} = -5.13$ eV, $\Delta\mu_S = 0$ eV), B ($\Delta\mu_O = -5.99$ eV, $\Delta\mu_{Zr} = 0$ eV, $\Delta\mu_S = -2.56$ eV), C ($\Delta\mu_O = -6.20$ eV, $\Delta\mu_{Zr} = 0$ eV, $\Delta\mu_S = -2.35$ eV), and D ($\Delta\mu_O = -3.75$ eV, $\Delta\mu_{Zr} = -4.70$ eV, $\Delta\mu_S = 0$ eV) is the chemical stability range of ZrOS. The line through points C and B corresponds to the maximally zirconium-rich conditions ($\Delta\mu_{Zr} = 0$ eV). Along lines parallel to C–B the zirconium chemical potential is constant.

Table 2

Structure relaxation of ions neighboring the vacancy site (only information for nearest neighbors (NN) is shown) ('-'/'+' means inward/outward displacement to the vacancy).

	V_O^0	V_O^{+1}	V_O^{+2}	V_{Zr}^0	V_{Zr}^{-1}	V_{Zr}^{-2}	V_{Zr}^{-3}	V_{Zr}^{-4}
For ZrO ₂								
NN _O	-0.083	-0.251	-0.241	0.141	0.146	0.153	0.157	0.163
NN _{Zr}	-0.028	0.194	0.196	-0.068	-0.075	-0.077	-0.082	-0.084
For ZrOS								
NN _O	0.028	0.044	0.064	0.138	0.133	0.127	0.123	0.120
NN _{Zr}	0.044	0.174	0.322	-0.050	-0.054	-0.059	-0.066	-0.086
NN _S	-0.108	-0.166	-0.282	-0.006	0.013	0.020	0.036	0.078

displacements of the zirconium (oxygen, and sulfur) atoms occupying the nearest-neighbor (NN) sites to the vacancy. For c-ZrO₂, it is shown that formation of the neutral oxygen vacancy (V_O^0) causes small (0.083 Å for O, and 0.028 Å for Zr) inward displacements of the neighboring zirconium and oxygen ions. Whereas, for positively charged oxygen vacancies (V_O^{+1} , and V_O^{+2}) the Zr ions near the vacancy displace outwards by 0.194–0.196 Å, this strong relaxation is caused by the fact that the neighboring Zr ions lose part of the screening effect provided by electrons in the neutral vacancy case. Formation of neutral zirconium vacancy (V_{Zr}^0) results in the repulsion felt by the oxygen ions and strong outward displacement (0.141 Å) of the neighboring oxygen ions. These results agree well with those reported for m-ZrO₂. [23] For ZrOS, the directions of atomistic displacement are the same with those for c-ZrO₂, but the absolute values of displacements are somewhat different. For instance, for V_O^{+2} in ZrOS Zr ions surrounding the vacancy displace outwards by 0.322 Å, which is 0.126 Å higher than that for c-ZrO₂.

The formation energies of oxygen and zirconium vacancies in c-ZrO₂ and ZrOS structures for two limiting values of oxygen chemical potentials (oxygen-rich limit ($\Delta\mu_O = -3.42$ eV) and oxygen-poor limit ($\Delta\mu_O = -5.99$ eV)) are shown in two forms: 1) at VBM ($E_f = 0$) (see Table 3); 2) as a function of the Fermi level (E_f) (see Fig. 3). In Fig. 3 the lowest limit of the Fermi level (E_f) represents the VBM, whereas the upper limit of E_f corresponds to the bottom of the calculated conduction band (BCCB). Only the vacancies among the lowest formation energies are shown. Due to the large formation heats of c-ZrO₂ and ZrOS structures defect formation energies strongly vary between the points A and B of the phase diagram (see Fig. 3). In both systems defect formation energies ($\Delta H_{D,q}$) become negative at some E_f which determines pinning energy (ϵ_{pin}) [58].

Next we analyze stability of oxygen and zirconium vacancies in c-ZrO₂. For oxygen-poor conditions, oxygen vacancy in doubly positively charged state (V_O^{+2}) is stable at $E_f < \epsilon_{pin}^+$. While increase of the Fermi level (E_f) to BCCB makes neutral oxygen vacancy the dominant defect. For these conditions formation of zirconium vacancies is unlikely due to high defect formation energy. Increasing the oxygen chemical potential reduces the stability of oxygen vacancies (increases their formation energy) and increases stability of zirconium vacancies (decreases their formation energies): V_O^{+2} still can form spontaneously near VBM, but for the higher Fermi level ($E_f > \epsilon_{pin}^+$) zirconium vacancies (V_{Zr}^{-4}) are stable. It should also be noted that oxygen vacancies in c-ZrO₂ show a “negative-U” behavior, in other words, V_O^{+1} is not stable against disproportionation into V_O and V_O^{+2} . For ZrOS structure, V_O^{+2} is also the most stable type of vacancies at VBM (see Table 3), and it can spontaneously form under oxygen-poor conditions (see Fig. 3). But, under oxygen-poor limit V_O^{+1} is stable in ZrOS structure at $0.46 \text{ eV} \geq E_f \geq 1.50 \text{ eV}$, while in c-ZrO₂ it is the metastable defect (see Fig. 3b). This suggests that the “negative-U” behavior is not typical for oxygen vacancies (V_O^0 , V_O^{+1} , and V_O^{+2}) in ZrOS. Similar to the c-ZrO₂, increasing the oxygen chemical potential can make V_{Zr}^{-4} stable close to BCCB. Analysis of Fig. 3 can also provide some information on the nature of oxygen and zirconium vacancies in c-ZrO₂ and ZrOS structures. For both structures, formation energy of oxygen vacancies increases with increasing

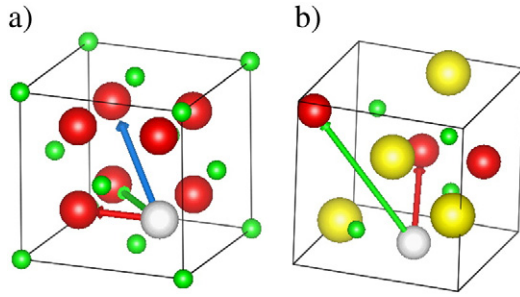


Fig. 4. a) Oxygen vacancy hopping along $\langle 100 \rangle$ (red color direction, Path 1), $\langle 110 \rangle$ (green color direction, Path 2) and $\langle 111 \rangle$ (blue color direction, Path 3) directions in $c\text{-ZrO}_2$; b) Oxygen vacancy hopping along Path 1 (red color direction) and Path 2 (green color direction) directions in ZrOS. The red spheres are O ions, green spheres are Zr ions and yellow spheres are S ions. White spheres are oxygen vacancies.

different types of vacancies can be stable at different range of Fermi level (E_f). However, E_f is not a free parameter and can be determined by the condition of charge neutrality (see Eq. 7, in other words, charged defects should compensate each other or should be compensated by doping)

$$\sum_i q_i C_i = 0 \tag{7}$$

where C is a defect concentration that is related to defect formation energy ($\Delta H_{D,q}$) through the equation

$$C(E_f, \mu, T) = N \exp\left(-\frac{\Delta H_{D,q}(E_f, \mu)}{k_B T}\right) \tag{8}$$

where N is a concentration of possible defect sites; T is temperature, k_B is the Boltzmann constant.

3.3. Migration of oxygen vacancies in ZrOS and $c\text{-ZrO}_2$ structures

Ionic conductivity (σ) of materials depends on defect concentration, defect formation energy ($\Delta H_{D,q}$), and migration barrier (E_m). It can be

expressed as an exponential function of the activation energy for defect diffusion (E_a) according to [59]

$$\sigma = \sigma_0 / T \exp\left(-\frac{E_a}{k_B T}\right) \tag{9}$$

where σ_0 is a temperature-independent prefactor. For low concentration of oxygen vacancies the activation energy is equal to the sum of the defect formation energy and the migration barrier ($E_a = \Delta H_{D,q} + E_m$).

Next, we compare migration barriers of doubly positively oxygen vacancies (V_O^{+2}) in $c\text{-ZrO}_2$ and ZrOS. For undoped $c\text{-ZrO}_2$, three possible migration pathways of oxygen vacancy exist (see Fig. 4a): oxygen vacancy hopping along $\langle 100 \rangle$ (Path 1), $\langle 110 \rangle$ (Path 2), and $\langle 111 \rangle$ (Path 3) directions. For Path 1, oxygen ion (vacancy) passing through a dumbbell of two zirconium cations in the middle of two tetrahedral oxygen sites. Analysis of the configuration for the saddle point (see Fig. 5) suggests that inter-atomic distance between the hopping oxygen ion and the zirconium ions is 1.967 Å (for $c\text{-ZrO}_2$ the equilibrium Zr-O is 2.211 Å), therefore for Path 1 migration barrier is determined by strong Coulombic attraction and large steric repulsion. Whereas, when oxygen ion hops via cation-anion pair (Path 2) or large interstitial space (Path 3), local electrostatic repulsion by surrounding anions leads to an increase in the migration barrier of the oxygen vacancy. Therefore, the lowest migration barrier of V_O^{+2} (0.282 eV) corresponds to Path 1 (see Fig. 5a). For the other pathways the V_O^{+2} migration barriers are significantly higher (see Table 4). These results agree well with the results predicted for CeO_2 [60], where it has been predicted that Path 1 has the lowest migration barrier. The lowest migration barrier predicted for $c\text{-ZrO}_2$ is within 0.05 eV of that for $t\text{-ZrO}_2$ [14].

For ZrOS, also several paths for the migration of oxygen ion exist (see Fig. 4b), however in all cases the oxygen vacancy migrates not through the Zr-Zr cation pair (which is the case for $c\text{-ZrO}_2$). Instead, it goes through the Zr-S pair (or even S-S pair). Therefore the lowest V_O^{+2} migration barrier (3.896 eV) is significantly higher than that for $c\text{-ZrO}_2$ (see Fig. 5b). Because of this and since equilibrium concentration of the charged oxygen vacancies in ZrOS is lower than that for $c\text{-ZrO}_2$, it becomes obvious that transition between ZrO_2 and ZrOS structures is accompanied by a decrease of the oxygen ionic conductivity. Moreover, it is well known that oxygen vacancies provide phonon scattering in ZrO_2 -based materials [3,61], which is necessary for

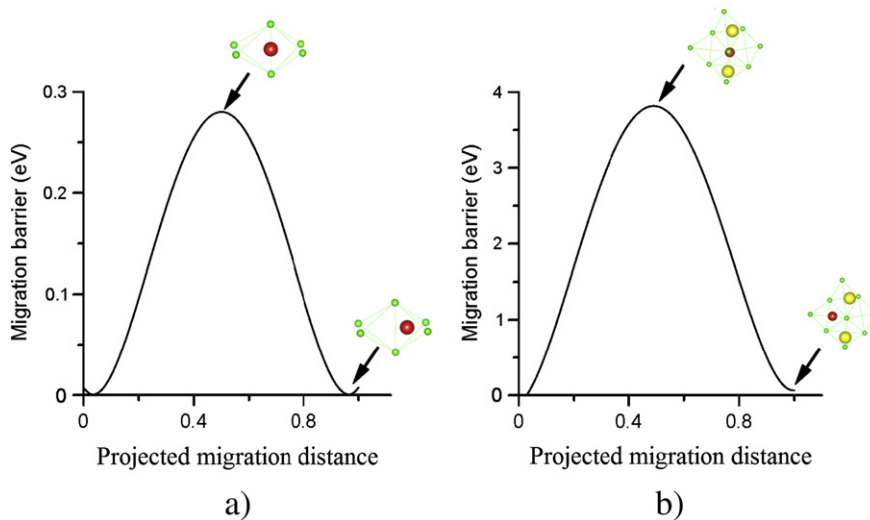


Fig. 5. Energy profiles during migration of doubly positively charged oxygen vacancies between two oxygen sites (a) in $c\text{-ZrO}_2$ and (b) in ZrOS, horizontal axis refers to projected migration distance. Initial and final positions of oxygen vacancy are referred as 0 and 1, respectively. Only pathways for the lowest migration barriers (Path 1 (see Fig. 4 for both $c\text{-ZrO}_2$ and ZrOS)) are shown.

Table 4

Calculated barriers (in eV) for the migration of doubly positively charged oxygen vacancies between different oxygen sites in pure *c*-ZrO₂ and ZrOS.

Structure	Diffusion/migration barriers (in eV)		
	Path 1	Path 2	Path 3
<i>c</i> -ZrO ₂	0.282	0.497	0.62
ZrOS	3.896	4.796	–

low thermal conductivity. Consequently, reduction of concentration of charged oxygen vacancies suggests that sulfur additions to zirconia may modify the thermal conduction of zirconia-based materials. Usually, under low sulfur partial pressure or extremely high oxygen pressure the effect of sulfur addition on vacancy formation and migration is small, since ZrOS is metastable. But the combination of the low oxygen and the high sulfur partial pressure may significantly limit the application of ZrO₂-based materials.

4. Conclusions

Based on density functional theory calculations, it has been shown that variation of the elemental chemical potentials can lead not only to the transition between zirconia (ZrO₂) and zirconium oxysulfide (ZrOS) phases, but also affect the stability and migration of intrinsic point defects. Analysis of defect formation energies in ZrOS and *c*-ZrO₂ shows that ZrO₂–ZrOS phases transition can significantly increase formation energy of doubly positively charged oxygen vacancies (V_O^{+2}) from -3.19 eV (for *c*-ZrO₂) to 0.61 eV (for ZrOS). This suggests that ZrOS is less prone to the formation of the charged oxygen vacancies than *c*-ZrO₂ under the same oxygen chemical potential conditions, but it is more prone to the formation of zirconium vacancies. Analysis of the defect mobility suggests that the lowest V_O^{+2} migration barrier is 3.614 eV higher in ZrOS structure than that in *c*-ZrO₂. Since oxygen vacancies play an important role in the ionic and thermal conductivities, these results indicate that sulfur additions to zirconia, either by doping or through gas diffusion, can change the conduction mechanisms of ZrO₂-based materials. This can significantly limit the possible applications of ZrO₂-based materials under high sulfur pressure, for instance, for nuclear reactors and SOFCs. Also, it can be stated that controlling the sulfur content in zirconia could change the conductivity of zirconia polymorphs. The computational schemes developed in this paper can also be used as a framework for evaluating the effect of different impurities on the stability of point defects in ceramic compounds.

Acknowledgment

Helpful discussions with Dr. Michael Sullivan from Institute of High Performance Computing (IHPC) of A*STAR in Singapore are highly appreciated. Computational support from IHPC is also gratefully acknowledged. Mr. OLEKSANDR I. MALYI is financially supported by Nanyang Technological University in the form of a Postgraduate Scholarship.

References

[1] J.J. Zhu, S. Albertsma, J.G. van Ommen, L. Lefferts, *J. Phys. Chem. B* 109 (2005) 9550–9555.
 [2] J. Kim, S. Lee, K.H. Kang, H.S. Hong, *Int. J. Energy Res.* 34 (2010) 438–444.
 [3] X.Q. Cao, R. Vassen, D. Stoever, *J. Eur. Ceram. Soc.* 24 (2004) 1–10.
 [4] N.Q. Minh, *J. Am. Ceram. Soc.* 76 (1993) 563–588.
 [5] A. Atkinson, S. Barnett, R.J. Gorte, J.T.S. Irvine, A.J. McEvoy, M. Mogensen, S.C. Singhal, J. Vohs, *Nat. Mater.* 3 (2004) 17–27.
 [6] R.M. Ormerod, *Chem. Soc. Rev.* 32 (2003) 17–28.
 [7] S.P. Jiang, S.H. Chan, *J. Mater. Sci.* 39 (2004) 4405–4439.

[8] D.G. Lamas, M.F. Bianchetti, M.D. Cabezas, N.E.W. de Reza, *J. Alloys Compd.* 495 (2010) 548–551.
 [9] H. Kim, C. Lu, W.L. Worrell, J.M. Vohs, R.J. Gorte, *J. Electrochem. Soc.* 149 (2002) A247.
 [10] M. Munoz, S. Gallego, J. Beltran, J. Cerda, *Surf. Sci. Rep.* 61 (2006) 303–344.
 [11] R.J. Ackermann, E.G. Rauh, C.A. Alexander, *High Temperature Sci.* 7 (1975) 304–316.
 [12] H.J.F. Jansen, J.A. Gardner, *Phys. B C* 150 (1988) 10–18.
 [13] C. Pascual, P. Duran, *J. Am. Ceram. Soc.* 66 (1983) 23–27.
 [14] A. Eichler, *Phys. Rev. B* 64 (2001) 174103.
 [15] X. Xia, R. Oldman, R. Catlow, *Chem. Mater.* 21 (2009) 3576–3585.
 [16] G. Katz, *J. Am. Ceram. Soc.* 54 (1971) 531.
 [17] J. Beltrán, S. Gallego, J. Cerdá, J. Moya, M. Muñoz, *Phys. Rev. B* 68 (2003) 075401.
 [18] J.I. Beltran, M.C. Munoz, *Phys. Rev. B* 78 (2008).
 [19] A. Christensen, E.A. Carter, *J. Chem. Phys.* 114 (2001) 5816.
 [20] S.V. Eremeev, S. Schmauder, S. Hocker, S.E. Kulkova, *Surf. Sci.* 603 (2009) 2218–2225.
 [21] C. Arhammar, C. Moysés Araújo, R. Ahuja, *Phys. Rev. B* 80 (2009) 115208.
 [22] J. Čížek, O. Melikhova, I. Procházka, J. Kuriplach, R. Kužel, G. Brauer, W. Anwand, T.E. Konstantinova, I.A. Danilenko, *Phys. Rev. B* 81 (2010) 024116.
 [23] A. Foster, V. Sulimov, F. Lopez Gejo, A. Shluger, R. Nieminen, *Phys. Rev. B* 64 (2001) 224108.
 [24] S. Kasamatsu, T. Tada, S. Watanabe, *Appl. Phys. Express* 2 (2009) 061402.
 [25] R. Platzter, E. Karapetrova, M.O. Zacate, J.A. Gardner, J.A. Sommers, W.E. Evenson, *Mater. Sci. Forum* 239 (1997) 57–60.
 [26] P.J. Shen, S.P. Jiang, K.P. Ong, W.Z. Ding, P.-L. Mao, X.G. Lu, C.H. Li, P. Wu, *J. Alloys Compd.* 506 (2010) 898–901.
 [27] J. Zheng, G. Ceder, T. Maxisch, W. Chim, W. Choi, *Phys. Rev. B* 75 (2007) 104112.
 [28] O.I. Malyi, Z. Chen, G.G. Shu, P. Wu, *J. Mater. Chem.* 21 (2011) 12363–12368.
 [29] J.X. Zheng, G. Ceder, W.K. Chim, *Phys. Status Solidi Rapid Res. Lett.* 2 (2008) 227–229.
 [30] A. Predith, G. Ceder, C. Wolverton, K. Persson, T. Mueller, *Phys. Rev. B* 77 (2008) 144104.
 [31] T. Sakuma, *J. Mater. Sci.* 22 (1987) 4470–4475.
 [32] S. Ostanin, E. Salamatov, A. Craven, D. McComb, D. Vlachos, *Phys. Rev. B* 66 (2002) 132105.
 [33] X.Y. Li, B. Hafskjold, *J. Phys. Condens. Matter* 7 (1995) 1255–1271.
 [34] F. Pietrucci, M. Bernasconi, A. Laio, M. Parrinello, *Phys. Rev. B* 78 (2008) 094301.
 [35] M. Kilo, R.A. Jackson, G. Borchardt, *Philos. Mag.* 83 (2003) 3309–3325.
 [36] A. Bogicevic, C. Wolverton, G. Crosbie, E. Stechel, *Phys. Rev. B* 64 (2001).
 [37] J.D. McCullough, L. Brewer, L.A. Bromley, *Acta Cryst.* 1 (1948) 287–289.
 [38] B.T. Kaminskii, G.N. Prokofeva, A.S. Plygunov, P.A. Galitskii, *Powder Metall. Met. Ceram.* 12 (1973) 521–524.
 [39] H. Zhang, B. Gao, B. Sun, G. Chen, L. Zeng, L. Liu, X. Liu, J. Lu, R. Han, J. Kang, B. Yu, *Appl. Phys. Lett.* 96 (2010) 123502.
 [40] R. Pornprasertsuk, P. Ramanarayanan, C.B. Musgrave, F.B. Prinz, *J. Appl. Phys.* 98 (2005) 103513.
 [41] R. Devanathan, W.J. Weber, S.C. Singhal, J.D. Gale, *Solid State Ionics* 177 (2006) 1251–1258.
 [42] J.P. Perdew, K. Burke, M. Ernzerhof, *Phys. Rev. Lett.* 77 (1996) 3865–3868.
 [43] P. Giannozzi, S. Baroni, N. Bonini, M. Calandra, R. Car, C. Cavazzoni, D. Ceresoli, G.L. Chiarotti, M. Cococcioni, I. Dabo, A. Dal Corso, S. de Gironcoli, S. Fabris, G. Fratesi, R. Gebauer, U. Gerstmann, C. Gougousis, A. Kokalj, M. Lazzeri, L. Martin-Samos, N. Marzari, F. Mauri, R. Mazzarello, S. Paolini, A. Pasquarello, L. Paulatto, C. Sbraccia, S. Scandolo, G. Sclauzero, A.P. Seitsonen, A. Smogunov, P. Umari, R.M. Wentzcovitch, *J. Phys. Condens. Matter* 21 (2009) 395502.
 [44] D. Vanderbilt, *Phys. Rev. B* 41 (1990) 7892.
 [45] H.J. Monkhorst, J.D. Pack, *Phys. Rev. B* 13 (1976) 5188–5192.
 [46] D.T. Hodul, A.M. Stacy, *J. Solid State Chem.* 62 (1986) 328–334.
 [47] C.G. Van de Walle, *J. Appl. Phys.* 95 (2004) 3851.
 [48] G. Makov, M.C. Payne, *Phys. Rev. B* 51 (1995) 4014–4022.
 [49] G. Henkelman, H. Jonsson, *J. Chem. Phys.* 113 (2000) 9978–9985.
 [50] G. Henkelman, B.P. Uberuaga, H. Jonsson, *J. Chem. Phys.* 113 (2000) 9901–9904.
 [51] S. Sayan, R.A. Bartynski, X. Zhao, E.P. Gusev, D. Vanderbilt, M. Croft, M. Banaszak Holl, E. Garfunkel, *Phys. Status Solidi B* 241 (2004) 2246–2252.
 [52] Q.B. Fan, F.C. Wang, H.L. Zhang, F. Zhang, *Mol. Simul.* 34 (2008) 1099–1103.
 [53] G. Lucovsky, J. Whitten, *Surf. Sci.* 601 (2007) 4138–4143.
 [54] P. Erhart, K. Albe, *J. Appl. Phys.* 102 (2007) 084111.
 [55] A. Terentjev, A. Catellani, G. Cicero, *Appl. Phys. Lett.* 96 (2010) 171901.
 [56] Z. Zhang, P. Wu, L. Lu, C. Shu, *Appl. Phys. Lett.* 88 (2006) 142902.
 [57] C. Loschen, J. Carrasco, K.M. Neyman, F. Illas, *Phys. Rev. B* 75 (2007) 035115.
 [58] R.N. Dominey, N.S. Lewis, M.S. Wrighton, *J. Am. Chem. Soc.* 103 (1981) 1261–1263.
 [59] D.A. Andersson, S.I. Simak, N.V. Skorodumova, I.A. Abrikosov, B. Johansson, *Proc. Natl. Acad. Sci. U. S. A.* 103 (2006) 3518–3521.
 [60] M. Nakayama, M. Martin, *PCCP* 11 (2009) 3241–3249.
 [61] D.R. Clarke, C.G. Levi, A.G. Evans, *Proc. Inst. Mech. Eng. A-J. Power Energy* 220 (2006) 85–92.
 [62] Z.T. Sui, X.Y. Xiao, K.Q. Huang, C.Z. Wang, *J. Less. Common. Met.* 163 (1990) 109–113.